nature neuroscience

Sodium pumps adapt spike bursting to stimulus statistics

Sara Arganda[1,2,4], Raúl Guantes[1,3,4] & Gonzalo G de Polavieja[1,2]

Pump activity is a homeostatic mechanism that maintains ionic gradients. Here we examined whether the slow reduction in excitability induced by sodium-pump activity that has been seen in many neuronal types is also involved in neuronal coding. We took intracellular recordings from a spike-bursting sensory neuron in the leech *Hirudo medicinalis* in response to naturalistic tactile stimuli with different statistical distributions. We show that regulation of excitability by sodium pumps is necessary for the neuron to make different responses depending on the statistical context of the stimuli. In particular, sodium-pump activity allowed spike-burst sizes and rates to code not for stimulus values *per se*, but for their ratio with the standard deviation of the stimulus distribution. Modeling further showed that sodium pumps can be a general mechanism of adaptation to statistics on the time scale of 1 min. These results implicate the ubiquitous pump activity in the adaptation of neural codes to statistics.

Adaptation to static stimuli is a well-known phenomenon in nervous systems. To understand the functions and mechanisms that are responsible for the flexibility of neuronal systems under real-world conditions, it is necessary to study adaptation to stimuli in their statistical context. Adaptation to the stimulus mean, the simplest parameter of a distribution, is a basic processing strategy in all sensory modalities that allows for sensitivity to fluctuations around the mean[1,2]. A more sophisticated strategy is the adaptation to the variance of the stimulus distribution[3–9] and perhaps to higher-order moments[10]. Stimulus variance also changes in time in natural conditions, and adapting to it allows the matching of output range to input range and a higher information transfer[7,8,11].

Despite the importance of adaptation to stimulus variance for the correct functioning of many systems, the underlying mechanisms of this adaptation remain largely unknown. Theoretical analysis and experimental evidence argue in favor of the existence of multiple mechanisms, which probably span several time scales and work under different constraints[12–20]. At the single-neuron level, current injection experiments have implicated slow sodium inactivation in bipolar cells[18,21] and sodium-dependent potassium conductances in cortex[20] as potential mechanisms.

The sodium-potassium ATPase, or sodium pump, is ubiquitous in neurons. During firing, Na^+ ions accumulate inside the axon, driving the sodium pump, which continues its activity even when the spike trains have ceased. The sodium pump exchanges three internal Na^+ ions for two external K^+ ions, and the resulting imbalance causes the membrane to recover from depolarization and can even hyperpolarize the membrane. The membrane hyperpolarization reduces membrane excitability, for example, in dopaminergic neurons[22], spinal networks[23], hippocampus[24,25], C-fibers in bullfrog sciatic nerve[26], insect mechanoreceptors[27] and human skin receptors[28].

We reasoned that the ability of the sodium pump to control excitability could, in principle, be a single-neuron mechanism for adaptation to stimulus variance. Although the faster dynamics of ion channels allow neurons to respond to particular stimulus features, the slow hyperpolarizing dynamics of sodium pumps effectively integrate past firing activity and affect future firing. Sodium-pump activity may then allow neurons to respond to stimulus features that are relative to the stimulus statistics. To test this hypothesis in a functionally relevant setting, we examined spiking receptors, which allow for naturalistic stimulation and minimize the interference from synaptic and network effects. For our experimental system, we used the skin deformation–receptor neuron in the leech, which is known as the T (tactile) neuron. The spike-receptor T neuron used to test this hypothesis responds to simple step stimuli on the skin with spike bursts. The advantage of this receptor neuron is that sodium pumps are known to control its excitability on the scale of 1 min[29–36], allowing for a clean test of our hypothesis that sodium-pump activity can adapt neuronal codes to stimulus statistics. In response to a train of action potentials, sodium-pump activity induces a hyperpolarization in this neuron of up to ~30 mV that lasts 1 min. Another hyperpolarizing current acting in this neuron is the calcium-dependent potassium current, which has a lower amplitude of up to 5 mV[30,37].

To study adaptation to stimulus variance, we first needed to determine the neuronal code. This is particularly notable in our case, as the neuron responds in bursts of spikes, which are thought to be a distinct mode of communication in sensory systems[38]. Bursts facilitate synaptic

[1]Neural Processing Laboratory, Instituto 'Nicolás Cabrera' de Física de Materiales, Facultad de Ciencias, C-XVI, [2]Department of Theoretical Physics, Facultad de Ciencias, C-XI, and [3]Department of Condensed Matter Physics, Facultad de Ciencias, C-III, Universidad Autónoma de Madrid, Madrid 28049, Spain. [4]These authors contributed equally to this work. Correspondence should be addressed to G.G.d.P. (gonzalo.polavieja@uam.es).

Received 20 June; accepted 20 August; published online 30 September 2007; doi:10.1038/nn1982

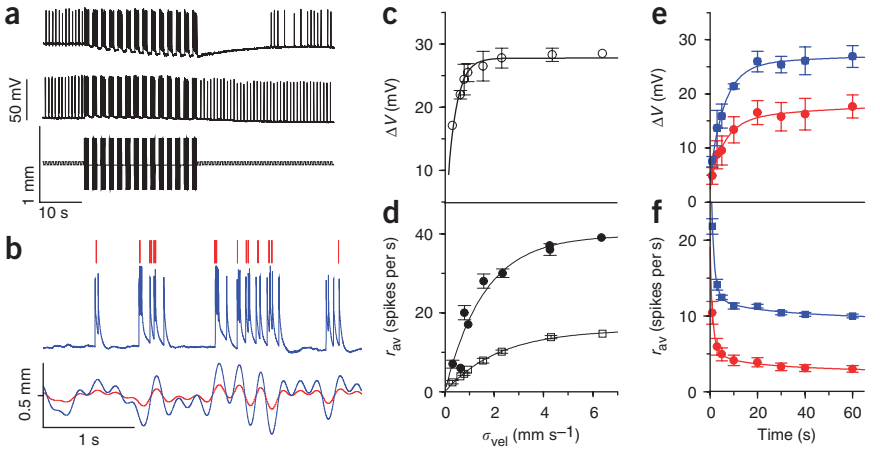

Figure 1 Reduction in membrane excitability with stimulus variance. (**a**) Top, response of the receptor neuron (T cell) to a protocol consisting of a 10-s train of 40-μm mechanical steps at 1.5 Hz on the skin of the leech, followed by 20 s of several 400-μm-amplitude sine-wave patterns at 10 Hz, and then repeating the initial train (bottom). Middle, response of same receptor neuron to same mechanical stimulation, but adding strophantidin to the bath solution. (**b**) Voltage response of mechanoreceptor (top) when the skin was stimulated with Gaussian white noise distributions of displacements with a cutoff frequency of 5 Hz and two different σ (bottom) (red line, $\sigma_{vel} = 0.75$ mm s^{-1}; blue line, $\sigma_{vel} = 2.25$ mm s^{-1}). (**c**) Decrease in membrane potential after 200 s of Gaussian white-noise stimulation as a function of σ_{vel}. (**d**) Average spike rate as a function of σ_{vel} (full circles represent average spike rate in the first second; empty squares represent the average firing rate after 10 min of stimulation). Solid lines are fits to exponential curves $y = a(1 - e^{-bx})$. (**e**,**f**) Dynamics of membrane voltage and average spike rate adaptation for the stimulus ensembles in **b** (red circles, $\sigma_{vel} = 0.75$ mm s^{-1}; blue squares, $\sigma_{vel} = 2.25$ mm s^{-1}). Solid lines are fits to a combination of exponential and power-law growth/decay, $y = a(1 - e^{-bx}) + cx^d$ and $y = ae^{-bx} + cx^d$, respectively. Error bars are s.d.

transmission, can improve the signal-to-noise ratio of responses and detect certain signals better than isolated spikes[38,39]. Another question about burst coding is which burst parameters are relevant for information transmission. Several proposals have been made, including spike frequency[40], burst duration[41,42] and latency of the first spike[43].

In this study, we have sought to determine what role, if any, the sodium pump has as a mechanism for adaptation to stimulus variance and its relevance for a burst code. First, we found that the sodium pump caused a greater hyperpolarization of the membrane for higher stimulus velocity variance. This hyperpolarization had the effect of decreasing excitability with increasing stimulus velocity variance. Second, we found that the neuron codes stimulus velocity into burst sizes and burst rates. Third, we determined that the hyperpolarization induced by sodium-pump activity had a notable impact on the neural code. The neuron does not code the stimulus velocity in bursts sizes and burst rates *per se*, but rather the velocity scaled by the standard deviation of the stimulus velocity distribution. This adaptive scaling was substantially disrupted in the presence of the sodium-pump blocker strophantidin. On the other hand, blocking the calcium-dependent potassium current with apamin did not significantly affect adaptational scaling ($P > 0.07$). A model of the receptor neuron further showed that sodium pumps alone can explain the observed adaptation to stimulus variance on the scale of 1 min.

RESULTS

Reduction in membrane excitability with stimulus variance

The sodium pump is responsible for adaptation on a slow time scale in the receptor neuron (**Fig. 1a**). We first examined the effect of the sodium pump in adaptation using a simple protocol for skin stimulation. Skin was subjected to a series of small (40-μm) mechanical steps at a frequency of 1.5 Hz both before and after 20 s of skin displacement that consisted of 400-μm amplitude sinusoidal patterns at 10 Hz (**Fig. 1a**, bottom). During the sinusoidal stimulation, the membrane hyperpolarized by 10 mV and did not respond to the following step stimuli for 20 s (**Fig. 1a**, top), except when we bathed the preparation with strophantidin (**Fig. 1a**, middle), a well-known blocker of the sodium pump[30,31]. The hyperpolarization that is induced by the pump activity after firing thus increases the voltage-to-spike threshold.

We next asked how the hyperpolarization and reduction in firing depended on the stimulus variance (**Fig. 1b–f**). It is illustrative to consider the raw spikes that are produced when the neuron is already adapted. The skin was stimulated with one of two Gaussian white-noise distributions of displacements with different standard deviation, σ, of 0.0425 mm (in velocity, $\sigma_{vel} = 0.75$ mm s^{-1}) or 0.1275 mm (2.25 mm s^{-1}) (**Fig. 1b**, red and blue lines, respectively). The neuron preferentially responded with spike bursts to slope in stimulus position (stimulus velocity), as occurred in the case of simple displacement step stimuli to which it responded only at stimulus onset and offset (**Supplementary Fig. 1** online). Notably, the firing characteristics for the two stimulus distributions were similar, despite their large difference in variance. This is possible because the neuron was more hyperpolarized for larger input velocity variance (23 mV and 27 mV for $\sigma_{vel} = 0.75$ and 2.25 mm s^{-1}, respectively), and therefore was in a state of reduced excitability. For the same value of input velocity, there was less response when the input distribution had larger velocity variance.

We then quantified the dependence of hyperpolarization and reduction of excitability on stimulus variance, (**Fig. 1c–f**). The hyperpolarization, ΔV, increased with increasing stimulus velocity s.d., σ_{vel}, up to a value of 28 mV at σ_{vel} of 3.25 mm s^{-1} (**Fig. 1c**). Reduction of excitability with increasing σ_{vel} was also apparent in the spiking rate that we obtained in the following manner. We calculated the initial average firing rate, r_{av}, for the first second of stimulation as a function of the σ_{vel} (**Fig. 1d**). The initial rate was higher with increasing σ_{vel} until a value of around 40 spikes per s at σ_{vel} of 3.25 mm s^{-1} (**Fig. 1d**, black points). We then calculated the average firing rate when the neuron was adapted after 10 min of stimulation. This rate was smaller and depended less on σ_{vel}, reaching a value of 13 spikes per s for $\sigma_{vel} > 2.25$ mm s^{-1} (**Fig. 1d**, white squares). The reduction of excitability could then be calculated as the difference between the initial spike rate and the spike rate when the neuron was adapted, $r_{av}(t = 1\text{ s}) - r_{av}(t = 10\text{ min})$, which increased with σ_{vel} and varied between 0 and 27 spikes per s. Neither hyperpolarization values nor reduction in excitability were found to depend substantially on the value of the cutoff frequencies used in the stimulus (5, 10 and 20 Hz in **Fig. 1**); instead they depended only on σ_{vel}. The dynamics of adaptation were on the order of 1 min for the range of the stimulus cutoff frequencies considered here, 5–20 Hz (**Fig. 1e,f**). At the start of stimulation, r_{av} was higher for larger σ_{vel}, as illustrated here for

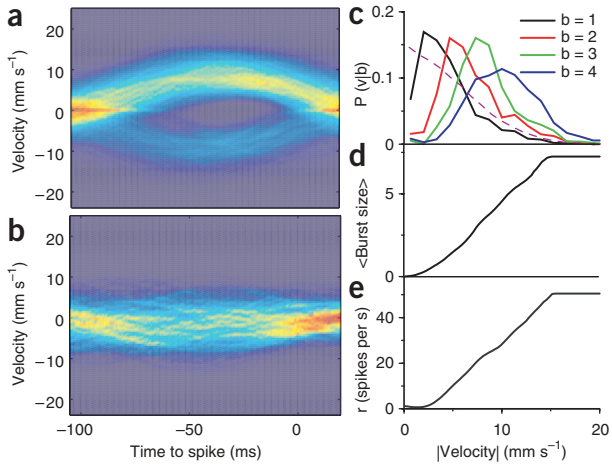

Figure 2 Burst size and rate code for mechanical velocity. (**a**) Velocity distribution before spike bursts in response to Gaussian white-noise stimulus (σ_{vel} = 3 mm s^{-1} and cutoff frequency of 5 Hz). (**b**) Velocity distribution before silences (intervals between bursts with at least 100 ms after/before spikes). (**c**) Velocity distributions calculated at the interval 5–25 ms before bursts of different sizes (black, single spikes; red, two-spike bursts; green, three-spike bursts; blue, bursts containing four or more spikes). Dashed line is the distribution of velocities in the stimulus ensemble. (**d**) Average burst size as a function of the stimulus velocity. (**e**) Burst rate as a function of the stimulus velocity.

two Gaussian distributions with a cutoff frequency of 5 Hz and σ_{vel} of 0.75 mm s^{-1} (red) or 2.25 mm s^{-1} (blue) (**Fig. 1f**). Spiking activity in turn activated the sodium pump, and the membrane hyperpolarized by values ΔV that were larger for the higher spike rates, that is, for larger stimulus velocity variance (**Fig. 1e**). Hyperpolarization then reduced excitability, as seen by the decay of spike rates over time (**Fig. 1f**). For the first 10 s there was an abrupt decay in the average spike rate, followed by a slower decay for approximately 1 min until stationary firing was reached.

Burst size and rate code for mechanical velocity

To determine how the sodium pump–induced hyperpolarization affects the coding properties of the neuron, we first sought to determine which code the neuron uses. In response to simple mechanical steps, the neuron responded to stimulus onset and offset, that is, to displacement changes or velocity (**Supplementary Fig. 1**). Using Gaussian white-noise stimuli, we found that stimulus velocity was encoded in spike-burst duration. Bursts were identified in the recordings using the distribution of interspike intervals (**Supplementary Fig. 1**, **Supplementary Note** and **Supplementary Table 1** online). We found that bursts were separated by at least 50 ms, a value that is very different from that of the intraburst time intervals, which have 10 ms as their most probable value. The distribution of velocity values before a burst of spikes peaked at a positive (entering the skin) velocity value and had a lower probability at negative (exiting the skin) velocity values (**Fig. 2a**). Compare this with the distribution before silences (intervals of velocity preceded or followed by at least 100 ms with no firing), which was similar to that of the original Gaussian stimulus centered at approximately zero velocity (**Fig. 2b**). There was an approximate symmetry in the velocity values that produced bursts when the skin was entering or exiting (**Fig. 2a**), and we thus, for simplicity, considered the absolute value of the velocity as the relevant coded variable. We carried out the same analysis for stimulus amplitudes and found no clear stimulus features that were responsible for bursting (**Supplementary Fig. 2** online). Longer bursts coded for higher velocities, as was seen in the velocity distribution before a burst of given size (**Fig. 2c**). The neuron responded to increasing stimulus velocity with bursts of increasing size, thus covering the tail of the stimulus velocity distribution (**Fig. 2c**, dashed line). Distributions (**Fig. 2c**) were calculated for illustrative purposes using the stimulus in the time interval of 5–25 ms before the first spike in the burst, but any fixed time or time intervals in the coding region of 5–40 ms before spiking gave similar results (**Supplementary Note** and **Supplementary Fig. 3** online). To study the ability of bursts to discriminate between values of stimulus velocity that were different from those corresponding to periods of no spiking, we carried out an analysis using an ideal-observer procedure (**Supplementary Note** and **Supplementary Fig. 4** online). We found that isolated spikes were poor at this discrimination task, whereas bursts of increasing size performed excellently. A similar burst-duration code has been predicted using biophysical models of cortical bursting neurons[44]. Although velocity was the more relevant variable coded for by bursts, using principal-component analysis we also found a small acceleration component (around 20% of total contribution to bursting versus 70% for the velocity component) to which the neuron was also sensitive (**Supplementary Note** and **Supplementary Fig. 5** online).

Once the relevant coded variables were determined, we quantified the response of the neuron in terms of these variables. We examined the neural gain, or nonlinear output, as a function of stimulus velocity (see Methods). Because we had found that burst duration was important for coding velocities, we first obtained the input-output relation for average burst size. The average burst size typically increased with stimulus velocity up to a saturation value (**Fig. 2d**). Burst size provided a good characterization of the response for the relevant range of input velocities, but we also checked whether other codes, such as the spike rate, were able to describe the neural gain as a function of velocity. Indeed, the spike rate was also found to be a relevant code. Bursts made two contributions to spike rate, one corresponding to the spike rate

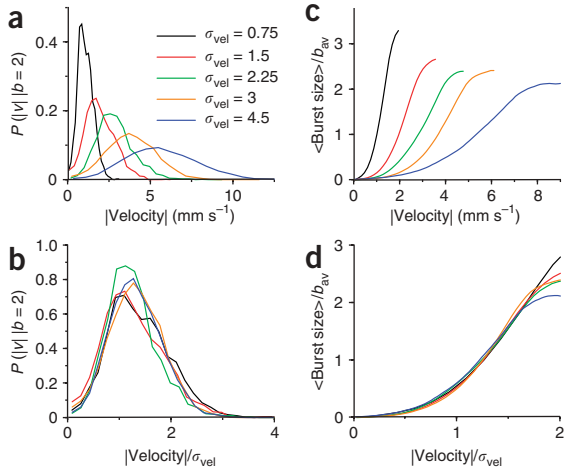

Figure 3 Adaptive rescaling in burst size. (**a**) Velocity distributions before bursts of two spikes for different stimulus ensembles (black line, σ_{vel} = 0.75; red, σ_{vel} = 1.5; green, σ_{vel} = 2.25; orange, σ_{vel} = 3; blue, σ_{vel} = 4.5 mm s^{-1}). Green and blue correspond to a cutoff frequency of 10 Hz and the rest correspond to a frequency of 5 Hz. (**b**) Velocity distributions as in **a**, but with velocity divided by σ_{vel}. (**c**) Average burst size as a function of stimulus velocity, normalized by the mean burst-size value at each stimulus σ. Stimulus ensembles and colors as in **a** and **b**. (**d**) Average burst size as a function of the stimulus velocity rescaled by the σ of the distributions.

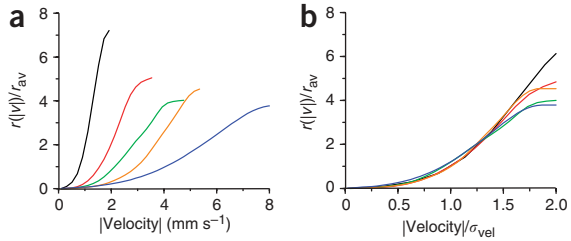

Figure 4 Adaptive rescaling in burst rates. (**a**) Burst rate as a function of the stimulus velocity, normalized by mean burst rate for different stimulus ensembles (black line, $\sigma_{vel} = 0.75$; red, $\sigma_{vel} = 1.5$; green, $\sigma_{vel} = 2.25$; orange, $\sigma_{vel} = 3$; blue, $\sigma_{vel} = 4.5$ mm s^{-1}). Green and blue correspond to a cutoff frequency of 10 Hz and the rest correspond to a frequency of 5 Hz. (**b**) Burst rate as in **a**, but with velocity divided by σ_{vel}.

within bursts and the other to the spike rate between bursts. The stimuli considered were very slow compared with intraburst times, so the spike rate within bursts cannot code for anything substantially different from burst duration. This leaves burst rate as the most relevant coding contribution to spike rate (**Fig. 2e**).

Burst size and burst rate adapt to stimulus variance

We have shown that stimulus velocity is coded for in burst size and burst rate, and that the effect of sodium pumps is to decrease excitability in proportion to stimulus velocity variance. How does this change in excitability affect coding? To answer this question, we next examined how the distribution of velocities before different burst sizes was affected by the decrease of excitability with increasing stimulus variance. Bursts of two spikes, for example, were produced in response to different velocity intervals depending on the variance of the stimulus distribution (**Fig. 3a**). The relevant scaling parameter was found to be the σ of the distribution of skin velocities. To examine this, we again plotted the probabilities (**Fig. 3a**), but this time for the ratio of the stimulus velocity to the σ of the total velocity distribution (**Fig. 3b**). The scaled probabilities were found to be independent of the stimulus variance. Bursts of a given size were then produced in response not to stimulus velocity, but to the ratio of velocity and the σ of the velocity distribution. Similar adaptive scaling was found for other burst sizes and even for isolated spikes (**Supplementary Fig. 6** online).

The same scaling was also found in the input-output functions. The average burst sizes in response to stimulus velocities were different depending on the stimulus variance (**Fig. 3c**). The same burst sizes, normalized by the mean burst duration, were instead produced in response to the ratio of velocity and σ of the stimulus velocity distribution (**Fig. 3d**). Burst rates showed the same scaling relationship (**Fig. 4**). Similarly to the case of normalized burst sizes (**Fig. 3c**,**d**), normalized burst rates for different input variances were elicited proportionally not to absolute velocity values (**Fig. 4a**) but to velocities that were relative to the σ of the input velocity distribution (**Fig. 4b**). Velocity is the most relevant variable that is coded, but is not the only one, and so we also tested whether there was adaptational scaling for other relevant stimulus features. To do this, we calculated the neural gain as a function of the two main stimulus filters obtained by principal-component analysis (**Supplementary Note**). These two filters corresponded to stimulus velocity and acceleration, and both showed a similar adaptation to variance (**Supplementary Fig. 5**).

Blocking sodium pumps disrupts adaptive scaling

Adaptation to statistics implies that a burst of given size is first produced in response to low velocities, but after 1 min of stimulation

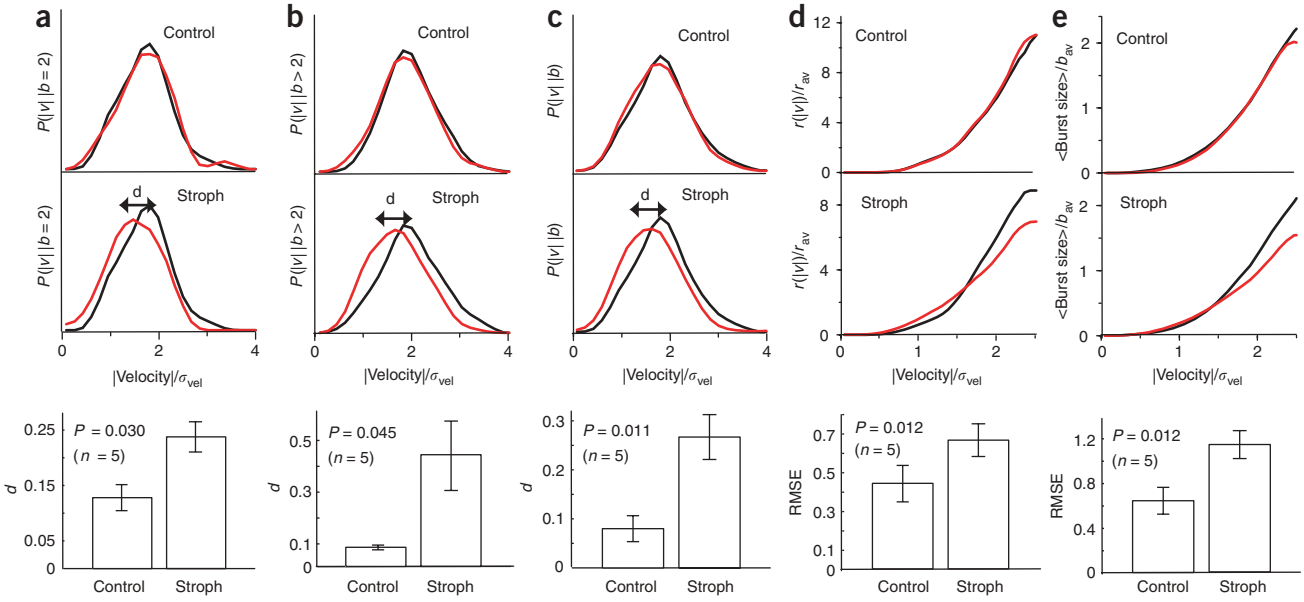

Figure 5 Blocking sodium pumps disrupts adaptive scaling. (**a**) Distribution of stimulus velocities scaled by the σ_{vel} before bursts of two spikes for two stimulus ensembles with σ_{vel} of 1.5 (black line) and 2.25 mm s^{-1} (red line) and a cutoff frequency of 5 Hz. Control experiments showed adaptive scaling (top), whereas the scaling was disrupted in the presence of strophantidin (middle). As a measure of disruption of adaptive scaling, the difference in the mean value of the two ensembles, *d*, was significantly larger in the presence of strophantidin (bottom). (**b**) Distribution of stimulus velocities as in **a**, but for bursts of three or more spikes. (**c**) Distribution of stimulus velocities as in **a**, but for all bursts. (**d**) Distribution of stimulus velocities as in **a**, but for normalized burst rates. As a measure of disruption of adaptive scaling, we used the root-mean-square error (RMSE) between the two curves, which was significantly larger for the strophantidin condition. (**e**) Distribution of stimulus velocities as in **d**, but for the normalized average burst duration. *P* values obtained from pair-wise *t*-tests after checking for Gaussianity (Lilliefors and Jarque-Bera tests) of the differences between controls and strophantidin conditions. Error bars are s.e.m.

it is produced in response to higher velocities. This implies that there is a shift of the response to higher velocities, higher the larger the stimulus variance. For a burst of three spikes, for example, the distribution of preceding velocities showed this shift to higher velocities (**Supplementary Fig. 7** online). After sodium pumps were blocked with strophantidin[30], there was at most 6–9 min of healthy firing response (see Methods), enough time to observe neither hyperpolarization nor a shift to higher velocities (**Supplementary Fig. 7**). Notably, there was a substantial disruption of adaptive scaling in the presence of the sodium-pump blocker strophantidin, shown for σ_{vel} of 1.5 (black) and 2.25 mm s^{-1} (red) (**Fig. 5**). This disruption of adaptive scaling was significant for all quantities implicated in the coding, including the distribution of velocities before bursts of two spikes (**Fig. 5a**, $P = 0.03$), bursts of three or more spikes (**Fig. 5b**, $P = 0.045$) and all bursts (**Fig. 5c**, $P = 0.011$), as well as the rate (**Fig. 5d**, $P = 0.012$) and average burst duration (**Fig. 5e**, $P = 0.012$). We tested that this disruption of adaptive scaling by strophantidin was not a result of additional nonstationary effects of the drug by checking that the input-output relationships were independent of the order of presentation of the stimulus distributions (**Supplementary Fig. 8** online).

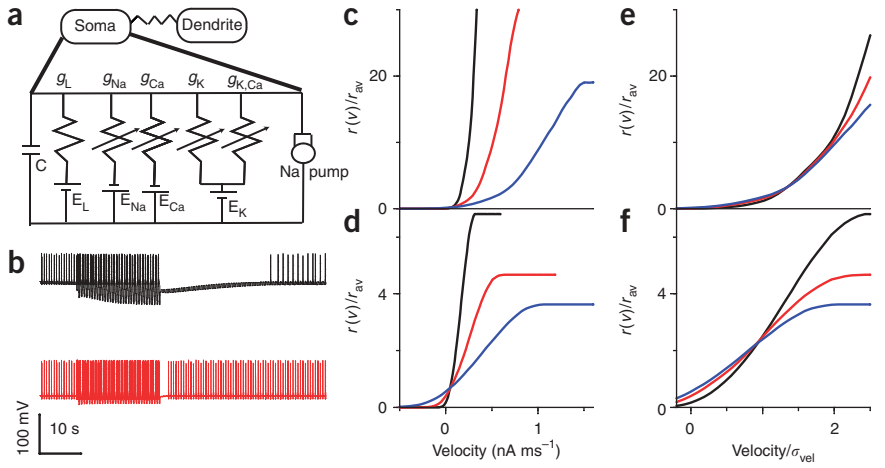

Figure 6 Sodium pumps responsible for adaptive rescaling in a neuron model. (**a**) Electrical circuit for each of the two compartments (soma and dendrite) of a leech T cell neuron model. Ionic conductances included leakage conductance (g_L), fast Na^+ conductance (g_{Na}), delayed rectifier K^+ conductance (g_K), high-threshold non-inactivating Ca^{2+} conductance (g_{Ca}), Ca^{2+}-activated K^+ conductance ($g_{K,Ca}$) and Na^+-activated pump current I_{pump}. (**b**) Black trace, neuron model response to a square wave stimulation (current step amplitude of 8 nA, period of 1.2 s) triggering 1 spike per period, followed by a sine wave with an amplitude of 40 nA and a frequency of 2 Hz producing higher activity. Red trace, response of the neuron model without the sodium pump. (**c**) Normalized burst rate for the model neuron in response to Gaussian white-noise current stimulation ensembles of different σ (black, 4.5 nA; red, 9 nA; blue, 18; cutoff frequency of 8 Hz). (**d**) Normalized burst rate as in **c**, but without the sodium pump. (**e**,**f**) Normalized spike rates in **c** and **d** with the input velocity rescaled by the σ of the input velocity ensemble.

Activity-induced hyperpolarization in this neuron is mainly due to the sodium pump, but to a lesser extent is also the result of a calcium-dependent potassium conductance with values up to 5 mV[30]. We therefore tested whether this potassium conductance has influences on adaptational scaling using the specific blocker apamin, which is known to inhibit the calcium-dependent potassium conductance in the T neuron[45] (see Methods). We found that in the presence of apamin the membrane hyperpolarized 4–5 mV less than it did in controls (**Supplementary Fig. 9** online), but with no significant effect on adaptive scaling (**Supplementary Fig. 10** online, $P > 0.05$).

Modeling sodium pumps as mechanism for adaptive scaling

We further investigated the role of sodium pumps in adaptational scaling using a two-compartment model. The model includes all known conductances for the T neuron (**Fig. 6a**, Methods and **Supplementary Note**; ref. 46). The responses of the model neuron to simple protocols that hyperpolarize the membrane were similar to those observed in experiments (**Fig. 6b**; compare with experiment in **Fig. 1a**). The small gap that we observed (**Fig. 6b**) is a result of the recovery time of the after-hyperpolarization conductance $g_{K,Ca}$, which has a faster time scale than that of the sodium pump[30,46]. The sodium pump has effects in both coding and adaptational scaling. Without the sodium pump, the neuron saturated earlier and thus did not code high velocities (**Fig. 6c** with pump, **Fig. 6d** without pump). Adaptational scaling took place in the complete model until velocities were twice the σ of the stimulus (**Fig. 6c**,**e**), which is similar to the experimental results (**Fig. 4**). The same model without sodium-pump dynamics showed no adaptive scaling in the normalized rate (**Fig. 6d**,**f**), which is similar to the experimental results (**Fig. 5d**). Similarly, we determined that in burst coding there was no adaptive scaling without sodium pumps, for example, in the distribution of stimulus velocities before bursts of two spikes (**Supplementary Fig. 11** online).

Eliminating the other hyperpolarizing conductance, the calcium-dependent potassium current, but retaining the sodium pump did not eliminate the adaptational scaling (**Supplementary Fig. 12** online), again reflecting the experimental results (**Supplementary Fig. 10**). Sodium pumps are therefore the only elements responsible for adaptational scaling in the model. We also used the model to test the generality of the effect and found that the hyperpolarization induced by sodium-pump activity might be larger for smaller neurons (**Supplementary Note** and **Supplementary Fig. 13** online).

DISCUSSION

We have shown both experimentally and using numerical simulations that sodium-pump dynamics are a mechanism for adaptation to stimulus variance on the time scale of 1 min. Our results consist of four parts. First, we dissected the coding properties of the bursting neuron and found that standard measures such as burst rates can be used as simple coding quantities. To further investigate the neural coding, we then showed that the neuron uses a burst code. Bursting has been found to be important in information transmission, as it improves synaptic reliability[41], the signal-to-noise ratio of neuronal responses[47] and the detection of behaviorally important features of the stimuli[39]. It is possible that bursts could act as unitary events or, alternatively, that their structures might convey extra information. Consistent with the second theory, it has been proposed that burst parameters are responsible for coding. Spike frequency during bursts might determine which postsynaptic neurons become excited[40]. Also, modeling studies of a general class of bursting neurons have shown that burst-duration codes for stimulus slope[44]. Experimental evidence that duration correlates with stimulus optimality in visual cortex[42] supports such a burst-duration code. Our experimental results are consistent

with the theoretical prediction of burst-duration coding slope, in our case the slope of skin displacements, with a larger slope in skin displacement corresponding with a longer burst. Second, our results show that the rate and burst codes show adaptive scaling. This further supports the relevance of burst size coding, as it shows the flexibility that is needed for changing real-world stimuli. In this manner the system can detect the velocity of approaching objects, with adaptive scaling allowing for the detection of high velocities relative to common stimuli such as water displacements. Third, we showed that blocking sodium pumps had a strong and significant disruptive effect on adaptive scaling. We also tested whether blocking the calcium-dependent potassium current had an effect on adaptive rescaling. No single statistical test showed a significant role for this current, but we found some evidence for it having a very weak effect on rescaling, close to statistical significance for bursts of two spikes. Finally, we modeled the neuron to further show that sodium pumps can be a general mechanism for adaptive scaling.

We expect sodium pumps to be important for adaptive scaling in other systems when tested with similar stimulations. Favorable preparations would be those in which hyperpolarization has already been shown to be induced by sodium-pump activity[22–28]. Both insect mechanoreceptors[27] and human skin receptors[28] are experimental systems similar to the one that we employed, and protocols very similar to ours could be directly adapted to these systems. In hippocampal pyramidal neurons there is a brief hyperpolarization of 1 s as a result of calcium-dependent potassium current and a hyperpolarization of 20 mV lasting 1 min that is due mainly to the sodium pump in normal conditions[24], similar to what occurs in the leech T neuron. In terms of functional relevance, this hyperpolarization in hippocampus may be seen as a way to avoid overexcitation[25], but more generally, it might scale neuronal responses to input statistics. When sodium-pump activity is reduced in hippocampal neurons, there is still hyperpolarization as a result of a sodium-sensitive potassium conductance[24]. The situation seems to be reversed in visual cortex, where there is hyperpolarization as a result of activity affecting a time scale of 30 s that is mostly due to a sodium-dependent potassium current, and in which sodium pumps might be of secondary importance[19]. Generally, sodium pumps and some potassium conductances might hyperpolarize the membrane on overlapping time scales in many neurons, with differences in their relative importance, as is the case in the T neuron, in hippocampus[24,25], in C-fibers in the bullfrog sciatic nerve[26], insect mechanoreceptors[27] and probably in visual cortex[19,20]. Adaptational scaling in bipolar cells in the retina has been shown to be due to slow sodium inactivation[18,21]. This is an effect that might be quite general on the time scale of 1 s, and that is, in principle, compatible with adaptational scaling on the scale of 1 min as a result of sodium-pump activity. Generally, adaptational scaling may have several single-neuron mechanisms acting on different time scales to cope with the complex dynamics of stimuli, as well as acting on the same time scale, probably to cope with different constraints such as allowing modulation by different molecular mechanisms.

METHODS

Experimental procedures. Adult leeches, *Hirudo medicinalis*, were bought from Zaug. We used semi-intact leech preparations that typically consisted of three or four ganglia (G7–G9/10) with intact connections from the central ganglia to their corresponding skin flaps. We recorded from a central ganglion and used the skin of the outer segments to pin the skin flaps to a Petri dish filled with Sylgard (Dow Corning). The extracellular solution contained 115 mM NaCl, 4 mM KCl, 1.8 mM $CaCl_2{\cdot}2H_20$, 1.5 mM $MgCl_2{\cdot}2H_20$, 10 mM glucose, 4.6 mM Tris maleate, 5.4 mM Tris base, and NaOH to a pH of 7.4 at room temperature (24–26 °C). To block sodium pumps, we bath applied 0.15 mM strophantidin in extracellular solution with 1% ethanol to better dissolve the drug[30]. The solution with the drug was first applied quickly using a pipette, and then afterwards applied at a constant flow of 1 ml min^{-1}. We tested that the drug was effective after 15 min using a protocol similar to the one in **Figure 1a**. Experiments with strophantidin used 3 min of white-noise stimulation for each variance and typically found 6–9 min of healthy firing. Before the addition of strophantidin, we carried out a control experiment in 1% ethanol using the same stimulation protocol. For these short recordings we used σ_{vel} of 1.5 and 2.25 mm s^{-1}, as larger variances are more likely to deteriorate the electrophysiology as a result of vibrations, and lower variances show more variability. To block the calcium-dependent potassium conductance, we used 1 nM apamin, which is known to block this conductance in the T neuron[45]. We observed its effect as a reduction of 5 mV in hyperpolarization (**Supplementary Fig. 9**). We obtained 10-min-long recordings for two stimulus variances in the presence of apamin. For a fair comparison between apamin and strophantidin conditions, statistical analysis was always carried out in the range of 0–2 scaled velocities, above which there are fewer data for analysis in short recordings. Microelectrodes were laser pulled using a P-2000 (Sutter Instruments) with inner and outer diameters of 0.5 and 1 mm, respectively, and backfilled with 4 M potassium acetate (Kach) to a final resistance of 40–70 MΩ. Amplification was achieved using an Axoclamp 1A amplifier and data was collected using a National Instrument card and custom-made data-acquisition software, created in MatLab, provided by M. Juusola (Univ. Sheffield). Mechanical stimulation of the skin was carried out using a closed-loop mechanical stimulator[48] (see ref. 49 for displacement and frequency distributions of the manipulator). Computer-aided stimulation was performed from above and approximately perpendicular to the skin using a 2.5-mm plastic ball that was held in contact with the skin. The ball was first pushed against the elastic skin so that the random displacements did not detach the ball from the skin and spikes were always produced in response to stimuli. We tested the skin's ability to follow the movement of the ball by increasing the stimulus velocity and keeping the amplitude constant, as more spikes would be elicited by following the different patterns in the stimulus. The stimulus range had a maximum of 1 mm with 0.1-μm resolution and a frequency range of 0–100 Hz. Pseudorandom stimuli with Gaussian distributions of displacements and a maximum frequency of 20 Hz were used.

Data analysis. Custom MatLab software was written for analysis. We separated bursts in the recording by the interspike-interval distribution (**Supplementary Note** and **Supplementary Fig. 1**). The stimulus-dependent bursting probability, $P(b|s)$, and bursting rate, $r(s)$, were obtained from Bayes' theorem,

$$P(b|s)/P(b) = P(s|b)/P(s)$$

where $P(s|b)$ was obtained from the recording by taking stimulus values before bursts. For long recordings, we took stimulus intervals by either using 20 ms (centered at $t = -15$ ms) before the onset of bursting or 20 ms around the maximum response, both of which corresponded to where the coding was more significant (**Supplementary Fig. 3**). Short recordings showed less variability using the second method, and were chosen for the statistical analysis in strophantidin and apamin conditions and their controls. $P(s)$ is the total stimulus distribution and $P(b)$ the average burst rate, typically written as r_{av}. The input-output relation for the average burst size (shown in **Fig. 2d** and **Fig. 3c,d**) was obtained as

$$\langle b(s)\rangle = \sum_n P(b = n|s)n$$

where $P(b = n|s)$is the stimulus-dependent probability for bursts of n spikes computed from Bayes' theorem. To further quantify the neuron's selectivity and coding properties, we used principal-component analysis and signal detection theory, respectively (**Supplementary Figs. 4** and **5**).

Computational models of T and bursting neurons. We modified a multicompartment model of the leech T neuron[46]. Our model contains two compartments, a soma and a dendrite (**Fig. 6a**). They consist of a membrane capacitance, C, of 1 μF cm^{-2} in parallel with two inward currents (a fast sodium current, I_{Na}, and a high-threshold Ca^{2+} current, I_{Ca}), an outward-persistent

potassium current, I_K, a leak current, I_L, and two currents that are solely regulated by intracellular Na^+ and Ca^{2+} pools, a Ca^{2+}-activated potassium current, $I_{K,Ca}$, and the sodium pump, I_{pump}. These last two currents are slow outward currents that are modulated by activity and are therefore responsible for different adaptation processes. $I_{K,Ca}$ is fast[46,50], and the slower I_{pump} is responsible for the long refractory times after sustained activity[46] (**Fig. 6b**). The differential equations for the time dependence of the membrane voltage in soma and dendrite are

$$-C\frac{dV_s}{dt} = I_L^s + I_{Na}^s + I_K^s + I_{Ca}^s + I_{K,Ca}^s + I_{pump}^s + g_c(V_s - V_d)/p$$

$$-C\frac{dV_d}{dt} = I_L^d + I_{Na}^d + I_K^d + I_{Ca}^d + I_{K,Ca}^d + I_{pump}^d + g_c(V_d - V_s)/(1-p) - I_{stim}$$

where the indices s and d stand for soma and dendrite, respectively, g_c is the electrotonic coupling and p is the ratio of soma to total membrane area. I_{stim} is the stimulation according to Gaussian white noise with a given frequency cutoff and variance. Details can be found in the **Supplementary Note**.

Note: Supplementary information is available on the Nature Neuroscience website.

ACKNOWLEDGMENTS

W. Kristan is gratefully acknowledged for support in the initial stages and M. Juusola for lending the mechanical stimulators and the MatLab-based BIOSYST program for data acquisition. F. Gabbiani is acknowledged for critical comments. Discussions with B. Burton, M. Fuenlazida, R. Harris, S. Laughlin, P. Lombardo and R. Scuri were also appreciated. We thank Ministerio de Educación y Ciencia, Spain (R.G., G.G.d.P.), Comunidad de Madrid-Universidad Autonoma de Madrid (G.G.d.P.), Comunidad de Madrid (BIOCIENCIA program) (G.G.d.P.), and a Comunidad de Madrid fellowship (S.A.) for financial support.

AUTHOR CONTRIBUTIONS

S.A. conducted experiments and performed significance tests, R.G. analyzed data, performed modeling and was responsible for writing parts of the supplementary information and G.G.d.P. conceived and directed the project, procured funding and wrote the paper.

Published online at http://www.nature.com/natureneuroscience
Reprints and permissions information is available online at http://npg.nature.com/reprintsandpermissions

1. Barlow, H.B. & Mollon, J.D. *The Senses* (Cambridge University Press, Cambridge, UK, 1982).
2. Walraven, J., Enroth-Cugell, C., Hood, D.C., MacLeod, D.I.A. & Schnapf, J.L. The control of visual sensitivity. in *Visual Perception: The Neurophysiological Foundations* (eds. Spillmann, L., Werner, J.S.) 53–101 (Academic Press, New York, 1990).
3. Shapley, R. Retinal physiology: adapting to the changing scene. *Curr. Biol.* **7**, R421–R423 (1997).
4. Meister, M. & Berry, M.J., II The neural code of the retina. *Neuron* **22**, 435–450 (1999).
5. Smirnakis, S.M., Berry, M.J., Warland, D.K., Bialek, W. & Meister, M. Adaptation of retinal processing to image contrast and spatial scale. *Nature* **386**, 69–73 (1997).
6. DeWeese, M. & Zador, A. Asymmetric dynamics in optimal variance adaptation. *Neural Comput.* **10**, 1179–1202 (1998).
7. Brenner, N., Bialek, W. & de Ruyter van Steveninck, R.R. Adaptive rescaling maximizes information transmission. *Neuron* **26**, 695–702 (2000).
8. Fairhall, A.L., Lewen, G., Bialek, W. & de Ruyter van Steveninck, R.R. Efficiency and ambiguity in an adaptive neural code. *Nature* **412**, 787–792 (2001).
9. Maravall, M., Petersen, R.S., Fairhall, A.L., Arabzadeh, E. & Diamond, M.E. Shifts in coding properties and maintenance of information transmission during adaptation in barrel cortex. *PLoS Biol.* **5**, e19 (2007).
10. Kvale, M.N. & Schreiner, C.E. Adaptation of auditory receptive fields to dynamic stimuli. *J. Neurophysiol.* **91**, 604–612 (2004).
11. Sharpee, T.O. *et al.* Adaptive filtering enhances information transmission in the visual cortex. *Nature* **439**, 936–942 (2006).
12. Abbott, L.F., Sen, K., Varela, J.A. & Nelson, S.B. Synaptic depression and cortical gain control. *Science* **275**, 220–224 (1997).
13. Tsodyks, M.V. & Markram, H. The neural code between neocortical pyramidal neurons depends on neurotransmitter release probability. *Proc. Natl. Acad. Sci. USA* **94**, 719–723 (1997).
14. Markram, H., Wang, Y. & Tsodyks, M. Differential signaling via the same axon of neocortical pyramidal neurons. *Proc. Natl. Acad. Sci. USA* **95**, 5323–5328 (1998).
15. Stemmler, M. & Koch, C. How voltage-dependent conductances can adapt to maximize the information encoded by neuronal firing rate. *Nat. Neurosci.* **2**, 521–527 (1999).
16. Fairhall, A. & Bialek, W. Adaptive spike coding. in *The Handbook of Brain Theory and Neural Networks* 2nd edn. (ed. Arbib, M.A.) 90–94 (MIT Press, Cambridge, 2002).
17. Gilboa, G., Chen, R. & Brenner, N. History-dependent multiple–time scale dynamics in a single-neuron model. *J. Neurosci.* **25**, 6479–6489 (2005).
18. Rieke, F. Temporal contrast adaptation in salamander bipolar cells. *J. Neurosci.* **21**, 9445–9454 (2001).
19. Sanchez-Vives, M.V., Nowak, L.G. & McCormick, D.A. Cellular mechanisms of long-lasting adaptation in visual cortical neurons *in vitro*. *J. Neurosci.* **20**, 4286–4299 (2000).
20. Sanchez-Vives, M.V., Nowak, L.G. & McCormick, D.A. Membrane mechanisms underlying contrast adaptation in cat area 17 *in vivo*. *J. Neurosci.* **20**, 4267–4285 (2000).
21. Kim, K.J. & Rieke, F. Slow Na^+ inactivation and variance adaptation in salamander retinal ganglion cells. *J. Neurosci.* **23**, 1506–1516 (2003).
22. Shen, K.Z. & Johnson, S.W. Sodium pump evokes high-density pump current in rat midbrain dopamine neurons. *J. Physiol. (Lond.)* **512**, 449–457 (1998).
23. Darbon, P., Tscherter, A., Yvon, C. & Streit, J. Role of the electrogenic Na/K pump in deinhibition-induced bursting in cultured spinal networks. *J. Neurophysiol.* **90**, 3119–3129 (2003).
24. Gustafsson, B. & Wigstom, H. Hyperpolarization following long-lasting tetanus activation of pyramidal hippocampal cells. *Brain Res.* **275**, 159–163 (1983).
25. Vaillend, C., Mason, S.E., Cuttle, M.F. & Alger, B.E. Mechanisms of neuronal hyperexcitability caused by partial inhibition of Na^+-K^+–ATPases in the rat CA1 hippocampal region. *J. Neurophysiol.* **88**, 2963–2978 (2002).
26. Kobayashi, J., Ohta, M. & Terada, Y. Evidence for the involvement of Na^+-K^+ pump and K^+ conductance in the posttetanic hyperpolarization of the tetrodoxin-resistant C-fibers in the islated bullfrog sciatic nerve. *Neurosci. Lett.* **236**, 171–174 (1997).
27. French, A.S. Two components of rapid sensory adaptation in a cockroach mechanoreceptor neuron. *J. Neurophysiol.* **62**, 768–777 (1989).
28. Kiernan, M.C., Lin, C.S. & Burke, D. Differences in activity-dependent hyperpolarization in human sensory and motor axons. *J. Physiol. (Lond.)* **558**, 341–349 (2004).
29. Baylor, D.A. & Nicholls, J.G. After-effects of nerve impulses on signalling in the central nervous system of the leech. *J. Physiol. (Lond.)* **203**, 571–589 (1969).
30. Jansen, J.K. & Nicholls, J.G. Conductance changes, an electrogenic pump and the hyperpolarization of leech neurons following impulses. *J. Physiol. (Lond.)* **229**, 635–655 (1973).
31. Van Essen, D.C. The contribution of membrane hyperpolarization to adaptation and conduction block in sensory neurones of the leech. *J. Physiol. (Lond.)* **230**, 509–534 (1973).
32. Scuri, R., Mozzachiodi, R. & Brunelli, M. Activity-dependent increase of the AHP amplitude in T sensory neurons of the leech. *J. Neurophysiol.* **88**, 2490–2500 (2002).
33. Scuri, R., Mozzachiodi, R. & Brunelli, M. Role for calcium signaling and arachidonic acid metabolites in the activity-dependent increase of AHP amplitude in leech T sensory neurons. *J. Neurophysiol.* **94**, 1066–1073 (2005).
34. Mar, A. & Drapeau, P. Modulation of conduction block in leech mechanosensory neurons. *J. Neurosci.* **16**, 4335–4343 (1996).
35. Catarsi, S. & Brunelli, M. Serotonin depresses the after-hyperpolarization through the inhibition of the Na^+/K^+ ATPase in the sensory neurones of the leech. *J. Exp. Biol.* **155**, 261–273 (1991).
36. Catarsi, S., Garcia-Gil, M., Traina, G. & Brunelli, M. Seasonal variation of serotonin content and non-associative learning of swim induction in the leech *Hirudo medicinalis*. *J. Comp. Physiol. A* **167**, 469–474 (1990).
37. Schlue, W.R. Effects of ouabain on intracellular ion activities of sensory neurons of the leech central nervous system. *J. Neurophysiol.* **65**, 736–746 (1991).
38. Krahe, R. & Gabbiani, F. Burst firing in sensory systems. *Nat. Rev. Neurosci.* **5**, 13–23 (2004).
39. Gabbiani, F., Metzner, W., Wessel, R. & Koch, C. From stimulus encoding to feature extraction in weakly electric fish. *Nature* **384**, 564–567 (1996).
40. Izhikevich, E.M., Desai, N.S., Walcott, E.C. & Hoppensteadt, F.C. Bursts as a unit of neural information: selective communication via resonance. *Trends Neurosci.* **26**, 161–167 (2003).
41. Lisman, J.E. Bursts as a unit of neural information: making unreliable synapses reliable. *Trends Neurosci.* **20**, 38–43 (1997).
42. DeBusk, B.C., DeBruyn, E.J., Snider, R.K., Kabara, J.F. & Bonds, A.B. Stimulus-dependent modulation of spike burst length in cat striate cortical cells. *J. Neurophysiol.* **78**, 199–213 (1997).
43. Middlebrooks, J.C., Clock, A.E., Xu, L. & Green, D.M. A panoramic code for sound location by cortical neurons. *Science* **264**, 842–844 (1994).
44. Kepecs, A., Wang, X.J. & Lisman, J. Bursting neurons signal input slope. *J. Neurosci.* **22**, 9053–9062 (2002).
45. Mozzachiodi, R., Scuri, R., Roberto, M. & Brunelli, M. Caulerpenyne, a toxin from the seaweed *Caulerpa taxifolia*, depresses afterhyperpolarization in invertebrate neurons. *Neuroscience* **107**, 519–526 (2001).
46. Cataldo, E. *et al.* Computational model of touch sensory cells (T cells) of the leech: role of the afterhyperpolarization (AHP) in activity-dependent conduction failure. *J. Comput. Neurosci.* **18**, 5–24 (2005).
47. Livingstone, M.S., Freeman, D.C. & Hubel, D.H. Visual responses in V1 of freely viewing monkeys. *Cold Spring Harb. Symp. Quant. Biol.* **61**, 27–37 (1996).
48. Chubbuck, J.G. Small-motion biological stimulator. *Johns Hopkins APL Technical Digest* **5**, 18–23 (1966).
49. Juusola, M. & French, A. The efficiency of sensory information coding in mechanical receptors. *Neuron* **18**, 959–968 (1997).
50. Wang, X.J. Calcium coding and adaptive temporal computation in cortical pyramidal neurons. *J. Neurophysiol.* **79**, 1549–1566 (1998).